Research article

Zhenming Wang, Jianxun Liu*, Xiaoguo Fang, Jiawei Wang, Zhen Yin, Huilin He, Shouzhen Jiang, Meng Zhao, Zongyou Yin, Dan Luo, Ping Shum and Yan Jun Liu*

Plasmonically enhanced photoluminescence of monolayer MoS_2 via nanosphere lithography-templated gold metasurfaces

https://doi.org/10.1515/nanoph-2020-0672
Received December 27, 2020; accepted March 9, 2021; published online March 24, 2021

Abstract: We demonstrate a simple, cost-effective method to enhance the photoluminescence intensity of monolayer MoS_2. A hexagonal symmetric Au metasurface, made by polystyrene nanosphere lithography and metal coating, is developed to enhance the photoluminescence intensity of monolayer MoS_2. By using nanospheres of different sizes, the localized surface plasmon resonances of the Au metasurfaces can be effectively tuned. By transferring monolayer MoS_2 onto the Au metasurface, the photoluminescence signal of the monolayer MoS_2 can be significantly enhanced up to 12-fold over a square-centimeter area. The simple, large-area, cost-effective fabrication technique could pave a new way for plasmon-enhanced light-mater interactions of atomically thin two-dimensional materials.

Keywords: metasurface; MoS_2; self-assembly; surface plasmon; photoluminescence.

1 Introduction

Atomically thin two-dimensional transition metal dichalcogenides (2D TMDCs) have been intensively investigated in recent years due to their unique physical and chemical properties [1–4]. With rapid development of nanofabrication and nanosynthesis techniques, their optical, electrical, electrochemical, and structural properties have been constantly improved [5–10]. Being a direct band gap semiconductor, monolayer (1-L) MoS_2 promises great potential for a wide range of applications such as field effect transistors [11], photodetectors [12, 13], and flexible electronics [14, 15]. However, due to its low dimension, the light–matter interaction for MoS_2 is extremely weak; in addition, the defects are inevitable during the process of fabrication. As a result, the quantum efficiency inside the MoS_2 is usually less than 1% [16, 17] and the photoluminescence (PL) of MoS_2 is extremely weak as well, limiting its potential applications to a great extent.

Various strategies have been put forward to enhance the PL emission of 2D TMDCs, which can be mainly divided into two categories: chemical treatment and physical assistance. Chemical treatment for the 1-L MoS_2 improves the PL intensity by fixing the atom vacancies and modifying the electron density [18–20]. By chemical treatment on 1-L MoS_2, the quantum efficiency can be improved to near unity from 0.6% and the PL intensity can experience an over 150 times enhancement. However, the chemically treated samples require extremely dry air environment, which is not favorable for the subsequent device fabrication and processing. Physical assistance mainly depends on the localized electromagnetic effects that can be created

*Corresponding authors: **Jianxun Liu**, Department of Electrical and Electronic Engineering, Southern University of Science and Technology, Shenzhen 518055, China; and **Yan Jun Liu**, Department of Electrical and Electronic Engineering, Southern University of Science and Technology, Shenzhen 518055, China; and Key Laboratory of Energy Conversion and Storage Technologies (Southern University of Science and Technology), Ministry of Education, Shenzhen 518055, China, E-mail: liujx@sustech.edu.cn (J. Liu); yjliu@sustech.edu.cn (Y. J. Liu). https://orcid.org/0000-0001-8724-0434
Zhenming Wang, Jiawei Wang, Zhen Yin, Dan Luo and Ping Shum, Department of Electrical and Electronic Engineering, Southern University of Science and Technology, Shenzhen 518055, China
Xiaoguo Fang and Huilin He, Department of Electrical and Electronic Engineering, Southern University of Science and Technology, Shenzhen 518055, China; Harbin Institute of Technology, Harbin 150001, China
Shouzhen Jiang, Shandong Provincial Key Laboratory of Optics and Photonic Device, School of Physics and Electronics, Shandong Normal University, Jinan 250014, China
Meng Zhao, Institute of Materials Research and Engineering, Agency for Science, Technology and Research (A*STAR), Singapore 138634, Singapore
Zongyou Yin, Research School of Chemistry, The Australian National University, Canberra, Australian Capital Territory 2601, Australia

by either plasmonic [21–29], dielectric [30–35] or metal-dielectric hybrid [36] nanoparticles/nanostructures. Comparatively, plasmonic nanomaterials provide large PL enhancement factor and wide tunability since the plasmonic resonances are highly dependent on the size, the shape and the spatial arrangement of nanoparticles/nanostructures. In particular, plasmonic metasurfaces (2D subwavelength metallic nanostructures) are highly advantageous due to their large-scattering cross section and local electromagnetic field enhancement near the surface of the metallic nanostructure. As a result, they can greatly enhance the light–matter interactions between the plasmonic metasurface and 2D TMDCs, leading to the enhanced PL emission [37]. As an ultrathin active layer, 2D monolayer TMDC becomes optically thick but physically thin to preserve the monolayer properties, thereby potentially leading to many optoelectronic applications with ultrathin, compact and integratable features.

However, due to the subwavelength feature of plasmonic metasurfaces, it still remains a grand challenge to achieve large-area, cost-effective fabrication strategy. Most of the state-of-the-art plasmonic metasurfaces have been made through the sophisticated nanofabrication techniques, such as electron-beam lithography (EBL), focused-ion beam (FIB) milling, self-assembly, etc. For examples, Butun et al. prepared Ag nanodisk arrays using EBL to enhance the PL intensity of 1-L MoS_2 [22]. By adjusting the size of Ag nanodisks (106–227 nm), the PL intensity was increased by 12 times. They proved that the PL enhancement came from the enhancement of the excitation field at the wavelength of pump laser and the effective scattering at the wavelength of exciton emission. Lee et al. proposed the MoS_2-Ag "bow-tie" resonant array system [23]. By adjusting the spacing of Ag nanoparticles in the silver-bowtie nanoantenna array, a strong coupling between MoS_2 excitons and the surface plasmons on the grid surface was achieved. Through localized surface plasmon resonance (LSPR) effect and Fano resonance, the PL intensity of 1-L MoS_2 had been increased by 40 times. More economical methods to enhance PL intensity were demonstrated by randomly attaching Au nanoparticles to TMDCs [24, 25]. Upon excitation, the created LSPRs from the Au nanoparticles will modify the local density of states of the TMDCs, hence causing the enhanced PL intensity. Although the PL of TMDCs can be largely enhanced via the random assembly of plasmonic nanoparticles, there is still room for improvement in terms of large-area uniformity and enhancement factor.

The aforementioned EBL and FIB techniques require complicated, costly processes and intensive, skillful labor, which are nonpreferred for large-area fabrication. Comparatively, self-assembly is a simple, cost-effective technique but lacks the accurate control of patterning, especially for plasmonic nanoparticles. Large-area self-assembly of polystyrene (PS) nanosphere can be achieved with the nanosphere size of 200 nm [38]. However, additional complicated surface modifications for colloidal nanosphere are required. In our previous report [39], we have developed an improved self-assembly method to obtain a large-area, high-quality monolayer PS nanospheres with simple additional steps compared to the conventional self-assembly method. By exploiting the monolayer PS nanospheres as a templated mask, we can fabricate a variety of periodic three-dimensional hierarchically ordered metastructures using cyclic inductively coupled plasma etching technique. In this work, hexagonal Au metasurfaces are fabricated using the nanosphere lithography technique, which is based on the templated masks via the self-assembled polystyrene nanospheres. By transferring the monolayer MoS_2 onto these Au metasurfaces, the PL signal of the monolayer MoS_2 can be significantly enhanced. Upon excitation by a 405 nm laser beam, the plasmonically enhanced monolayer MoS_2 exhibits a 12-fold increase in PL intensity over a large area. Experimental results show that our proposed approach is a simple, large-area, and cost-effective fabrication technique, which could pave a new way for plasmon-enhanced light-mater interactions such as photoexcitation and nonlinear optics of 2D TMDCs.

2 Materials and methods

2.1 Templated masks preparation

The PS nanosphere latex solutions (2.5 wt% dispersion in water) with different nanosphere sizes in diameter (350, 400, 500, 600, and 750 nm) were purchased from Alpha Aesar Chemical Co., LTD (Shanghai, China) and Shanghai Aladdin Bio-Chem Technology Co., LTD (Shanghai, China). Prior to making templated masks by nanosphere self-assembly, the glass substrates were subsequently cleaned with acetone, ethanol, isopropanol and deionized (DI) water in an ultrasonic cleaner (KQ-250DE, Kun Shan Ultrasonic Instruments Co., Ltd), and then followed by 15 min treatment in a UV-O_3 cleaner (BZS250GF-TC, HWOTECH). The templated masks for nanosphere lithography consisted of a monolayer of PS nanospheres, which were formed on the glass substrate via an improved self-assembly method at the air–liquid interface [33].

2.2 Gold metasurface fabrication

Once the monolayer-PS-nanosphere templated masks were ready, a 2 nm thick Cr layer and a 50-nm-thick gold film were sequentially deposited on the templated masks by an electron-beam evaporator (TF500, British HHV). The ultrathin Cr film served as an adhesion layer

in our experiments. To reduce the surface roughness and strengthen the adhesion of the Au film simultaneously, the evaporation rates in the deposition process were controlled to be ~0.2 Å/s for the Cr film and ~0.5 Å/s for the Au film, respectively. During the deposition process, the vacuum level inside the evaporator chamber was controlled at 5×10^{-6} Torr. After deposition, the Au-coated templated masks were soaked into the DI water to remove the PS nanospheres with the help of ultrasonic cleaner. The removing process was carried out at the power of 90 W and lasted for 1 min. Finally, we achieved the gold metasurface on the glass substrates.

2.3 Transfer of 1-L MoS_2

The CVD-grown 1-L MoS_2 samples on the Si substrates (SIX-Carbon Inc., China) were used in our experiments. The MoS_2 was a continuous film with a size of 1×1 cm^2, which can be easily stripped off from the Si substrate without any additional treatment. The Si substrate with the 1-L MoS_2 was slowly immersed into the DI water with a tilt angle of ~45°. Due to the surface tension of water, the 1-L MoS_2 atomic film separated from the Si substrate and then floated on the water surface. Meanwhile, the Si substrate sunk into the water bottom. After that, the hydrophilically treated Au metasurface was used to pick up the floating MoS_2 film. We immersed the target substrate into the DI water, kept an angle of ~45° with respect to the water surface, and pick up the MoS_2 film gently. Please also refer to the supplementary videos of the transfer process in the supporting information.

2.4 Characterization and measurements

Surface morphologies of the Au metasurfaces were investigated using the field-emission scanning electron microscopy (FESEM, Merlin, Zeiss) and atomic force microscope (AFM, Ahpha300, WITec). The optical spectra of the Au metasurfaces were collected by a UV-Vis-NIR microspectrophotometer (CRAIC technologies Inc.). We carried out the Raman spectra measurement and Raman mapping to confirm the transferred 1-L MoS_2 on the gold metasurface using a confocal Raman system (Alpha300, WITec). We used a 100× objective lens to focus the excitation laser light (working wavelength: 532 nm) onto the samples and collect the Raman signal to the spectrometer. For PL test, a laser with the working wavelength of 405 nm was used for the MoS_2 excitation, and a 100× objective with the numerical aperture of 0.8 was used to focus the laser beam onto the 1-L MoS_2 sample and collect the emitted PL signals simultaneously. A 450 nm long-pass filter was put in the PL collection light path to block the reflected laser light. The PL spectra were measured under a microscopy-combined spectrometer system (MA 01720, Princeton Instruments). To ensure the repeatability of the PL spectra and exclude the subtle differences between different areas on each sample, the PL signal was taken and averaged at randomly selected 10 positions within an area of 1×1 cm^2 on every single sample under the same experimental conditions.

2.5 Simulation

The optical fields and transmission spectra were calculated using the finite-difference time-domain (FDTD) method. The dispersion of gold is based on Johnson and Christy model. The simulation area was set to allow only one period of the gold metasurface in the *x*-*y* plane and enough space for the light source and power monitors. Auto-uniform meshing with the finest meshes (2 nm minimum mesh step) was used to achieve the accurate results. The light source was selected with the wavelengths ranging from 400 to 1300 nm. Three power monitors were separately located 5 nm above the Au metasurface, 1 μm above the light source and 3 μm below the gold metasurface to collect electric field intensity, reflected and transmitted optical signals.

3 Results and discussion

Figure 1a is a schematic illustration of the 1-L MoS_2-covered Au metasurface. The surface morphologies of all the metasurfaces fabricated from the templated masks using the PS nanospheres with different sizes (350, 400, 500, and 600 nm in diameter) have been characterized under the SEM, as shown in Figure S1. As mentioned above, we used continuous monolayer MoS_2 rather than single crystalline one during the transfer process. Such a large-scale, CVD-grown MoS_2 monolayer covers the Au metasurface evenly. In addition, there was no requirement of a support layer during the wet transfer, hence avoiding pollution effectively [40]. The purchased 1-L MoS_2 samples and the fabricated metasurfaces were characterized using AFM, as shown in Figure S2. The measured thicknesses of 1-L MoS_2 and metasurfaces are ~1 and ~50 nm, respectively. Figure 1b shows the optical image of 1-L MoS_2-covered Au metasurface, where the metasurface was fabricated from the templated mask using the PS nanospheres with the diameter of 750 nm. A clear boundary of the MoS_2 is marked by the black dashed line.

During the transfer process, the 1-L MoS_2 could be folded, stacked or damaged due to improper handling. To ensure that the transferred MoS_2 was still a monolayer, we carried out Raman spectra measurement on the transferred samples. As known, for the 1-L MoS_2, the E^1_{2g} (in plane) and A_{1g} (out of plane) are the main vibration modes that locate at ~384 and ~403 cm^{-1}, respectively [41, 42]. Depending on the experimental environment, the specific positions of these two characteristic Raman peaks of 1-L MoS_2 might be slightly different, however, their spacing is usually fixed. Figure 1c shows the Raman spectra of 1-L MoS_2 transferred onto the Au metasurface. We can see that after transfer, the wavenumber spacing between the A_{1g} and E^1_{2g} modes still remains 18 cm^{-1}, confirming that the transferred MoS_2 onto the Au metasurface is still a monolayer. In order to verify that the 1-L MoS_2 transferred onto Au metasurface still remains good quality, a 10 × 10 μm^2 Raman mapping covering the boundary was carried out, as shown in Figure 1d. The continuity and integrity of transferred 1-L MoS_2 can be directly resolved by the distribution and variation of the A_{1g} signal intensity. In the mapping results, the distribution of A_1 peak and E^1_{2g} peak are almost the same.

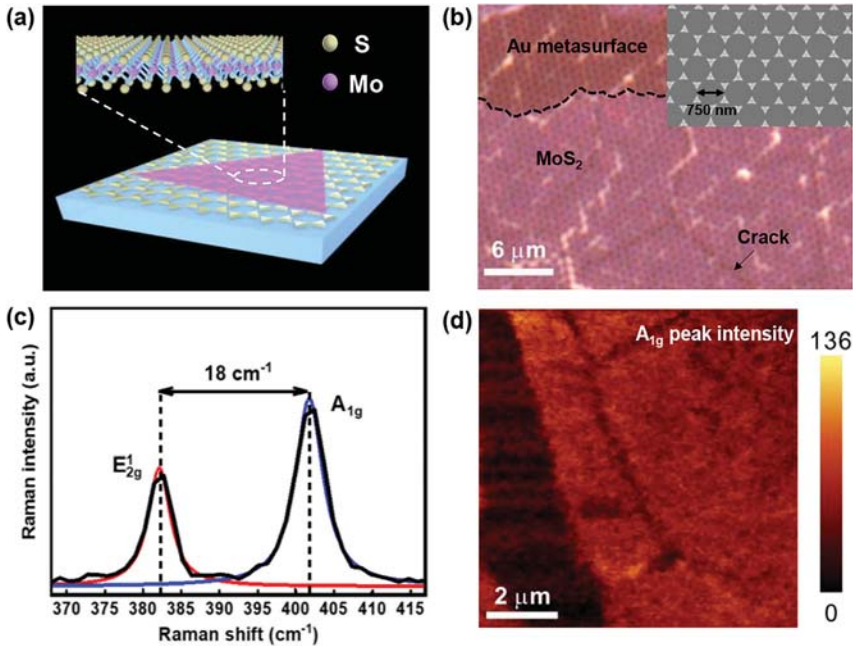

Figure 1: (a) Schematic of a 1-L MoS_2-covered Au metasurface on a glass substrate, and the crystal structure of 1-L MoS_2 is shown in the inset. (b) Optical image of 1-L MoS_2-covered Au metasurface. A clear boundary of the MoS_2 is marked by the black dashed line. The arrow points out the crack on MoS_2. Inset shows a typical SEM image of the Au metasurface fabricated from the templated mask using the PS nanospheres with the diameter of 750 nm. (c) Raman spectra of MoS_2 transferred onto metasurface. With the peaks fitting, the Raman shift between A_{1g} mode and E^1_{2g} remains 18 cm^{-1}. (d) Raman mapping for boundary area with the collected signal of A_{1g} peak.

The fabricated Au metasurfaces consist of hexagonally arranged triangle prisms. Each triangle prism is expected to produce strong LSPRs upon excitation, which will then enhance the absorption and emission efficiency of the 1-L MoS_2. In our study, we fabricated the Au metasurfaces with different periods and unit sizes, which were highly dependent on the templated masks by the self-assembled nanospheres of different sizes. It is straightforward that the LSPRs of Au metasurfaces are highly dependent on structural parameters. Figure 2 shows the measured and simulated spectra of the Au metasurfaces that were fabricated from the templated masks with different nanosphere sizes (350, 400, 500, 600, and 750 nm in diameter). From the simulated results in Figure 2d, for the Au metasurface made by nanospheres with the size of 350 nm, the absorptance peak locates ~670 nm. With the nanosphere diameter changing from 350 to 750 nm, the period of the Au metasurface increases, and the individual Au unit structure becomes large as well (see Figure S1). As a result, the absorptance peaks of the Au metasurfaces demonstrate a clear red shift from ~670 to ~1200 nm, showing a broad absorption tuning range. Meanwhile, the transmittance and the reflectance spectra exhibit the similar trend as the absorptance ones. The experimental results are also in reasonable agreement with

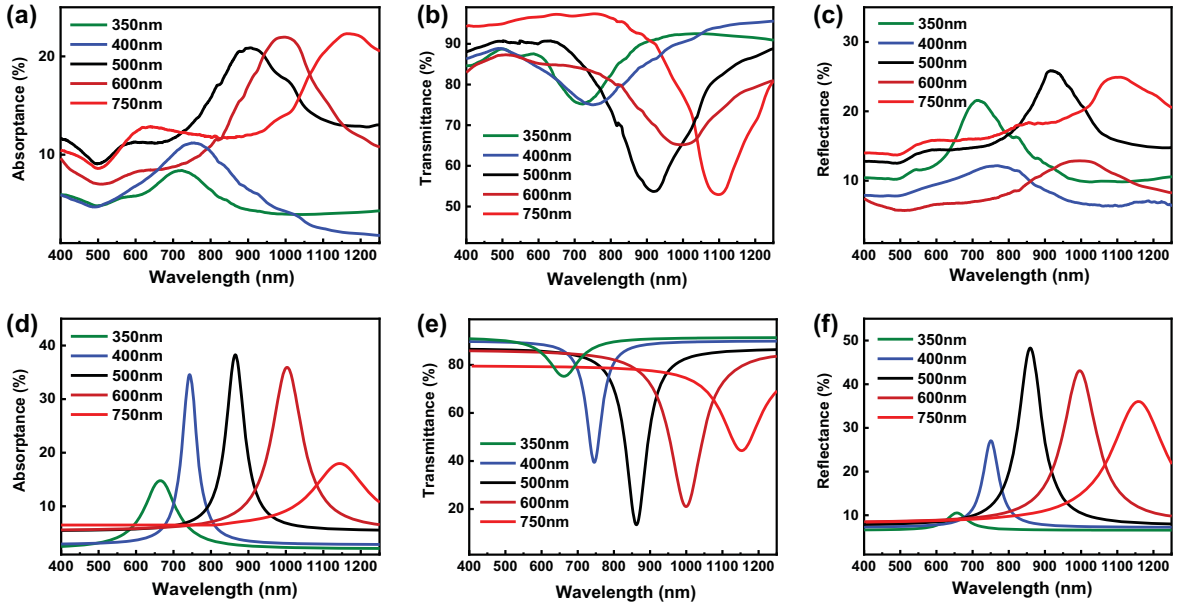

Figure 2: Measured (a–c) and simulated (d–f) absorptance (a, d), transmittance (b, e), and reflectance (c, f) spectra of the Au metasurfaces.

the simulation and show a similar trend as the simulated results. It is worth mentioning that there are also discrepancies between experimental and simulated results, which could be mainly attributed to the fabrication errors and the defects in the fabricated samples.

We subsequently investigated the effect of Au metasurfaces on the PL emission using a semiconductor laser (405 nm) as the pumping source. We pumped the 1-L MoS_2-covered Au metasurfaces at various pumping intensities. As a control experiment, we also studied the PL of the nontransferred 1-L MoS_2 as a function of excitation laser intensity, as shown in Figure 3a. It can be clearly seen that as the laser intensity increases, the PL intensity becomes strong. The primary PL peak locates at 672 nm. At a higher excitation intensity, we also notice an emergence of a secondary PL peak, locating at ~620 nm. It is well-known that these two main peaks locating at 672 and 623 nm correspond to the A1 and B1 band transitions of 1-L MoS_2 [43, 44]. Compared to B1 band transition related to E^1_{2g} (in plane) mode, A1 band related to A_{1g} (out of plane) transition has higher PL intensity and more sensitive to the Au metasurface [18]. Figure 3b shows measured PL intensity of the 1-L MoS_2 on the Au metasurfaces that were fabricated from self-assembled nanospheres with different sizes at a fixed pumping intensity. At the fixed pumping intensity of 7.8 mW/cm^2, compared Figure 3b to Figure 3a, there is significant enhancement of A–exciton emission due to the addition of the Au metasurface compared to the nontransferred sample. It can be also clearly seen from Figure 3b that as the size of the PS nanospheres decreases, the PL enhancement becomes significantly prominent. In addition, the secondary PL peak at ~620 nm (corresponding to B-exciton emission) has been greatly suppressed, which might be attributed to the absorption of Au metasurfaces.

The PL spectra of the 1-L MoS_2 on different Au metasurfaces under various pumping intensities have been also investigated and the results are summarized in Figure S3. From Figure S3 and Figure 3b, we can see that there is different enhancement of PL signals for each Au metasurface. It is obvious that among the Au metasurfaces in our experiments, the one made by nanospheres with the size of 350 nm in diameter provides the largest enhancement. To directly illustrate the enhancement effect of Au metasurface, we have plotted the PL peak intensity as a function of the excitation laser intensity, as shown in Figure 3c. It is obvious that for all cases, the PL peak intensity consistently changes linearly with the excitation laser intensity. Therefore, with the PL intensity of the nontransferred case as a baseline, the slope of each fitting line indicates the enhancement factor provided by the Au metasurfaces.

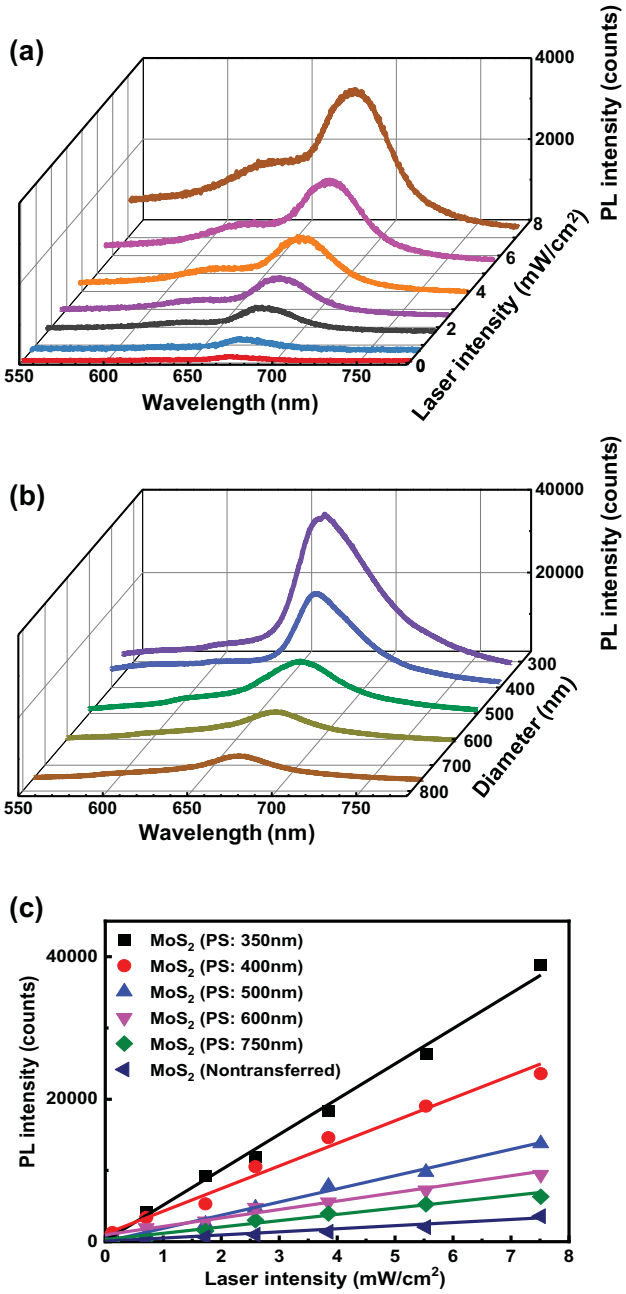

Figure 3: The measured PL signals of (a) the nontransferred 1-L MoS2 as a function of the pumping laser intensity (0.8–7.8 mW/cm^2), and (b) the transferred 1-L MoS2 on different Au metasurfaces made by the nanospheres with different sizes in diameter (350–750 nm) under the fixed pumping laser intensity of 7.8 mW/cm^2. (c) The scatter plot for the PL intensity of A-exciton in 1-L MoS2, including samples nontransferred and samples transferred onto various metasurface. The straight line in the figure is the result of linearly fitting for the spots in the scatter plot. The color of the line corresponds to the color of the fitted spots.

The enhanced PL from the 1-L MoS_2 could be attributed to the enhanced absorption or emission or both. Upon the laser excitation, the Au metasurfaces could be resonantly

excited. As a result, strong LSPRs are induced around each unit, producing a large $|E|^2$ near the 1-L MoS_2 and subsequently enhancing the absorption efficiency of the 1-L MoS_2. On the other hand, the strong LSPRs could also modify the local density of states in the 1-L MoS_2 due to the well-known Purcell effect [45–47], resulting in an additional emission pathway for the MoS_2 and further enhancing PL. We also derived enhancement factor of each Au metasurface from the slopes of each fitting line, as shown in Figure 4a. Among the investigated Au metasurfaces in our experiments, we can see from Figure 4a that as the nanosphere diameter increases, the enhancement factor gradually decreases. In our experiments, the Au metasurfaces made by the nanospheres with the size of 350 and 750 nm provide the maximum and minimum enhancement factors (i.e., 12× and 2×), respectively. We have also numerically calculated the local field enhancement of the Au metasurfaces under the excitation and emission wavelengths (405 and 677 nm, see Figure 4b and c), respectively. The calculation details can be found in the supporting information. We have also numerically calculated the near-field electric field distributions of the Au metasurfaces at the excitation and emission wavelengths, as shown in Figure S4 in the supporting information. From Figure S4, we can confirm that the PL enhancement mainly arises from single Au triangle plasmonic modes rather than the coupling effect between two triangle prisms because the triangles are spaced too far to form strong couplings. It is worth noting that the gap between the adjacent triangles can be further tuned via etching nanosphere first before the gold film deposition [48]. By precisely controlling the gap size, strong plasmonic couplings can be achieved to further enhance the PL signal. It is also worth mentioning that we only numerically calculated local field enhancement around the Au triangles in the Au metasurfaces at the excitation and emission wavelengths in Figure 4b and c, meaning that we neglected the other areas where there are no Au triangles in the Au metasurfaces. From the SEM images of Au metasurfaces in Figure S1, the Au triangles only account for a small fraction of the whole metasurface area. As a result, the achieved enhancement factor becomes smaller by taking into account of PL contribution from the whole area of Au metasurface. As shown in Figure 4b and c, $|E_{avg}|^2$ decreases as the nanosphere diameter increases for both excitation and emission wavelengths. Interestingly, $|E_{avg}|^2$ for both cases experiences the coincidently same trend as the measured enhancement factor, indicating that the strong LSPRs generated from the Au metasurfaces indeed enhance both absorption and emission of the 1-L MoS_2. From Figure 4, we could foresee that as the nanosphere size further decreases, the enhancement factor will become larger. For example,

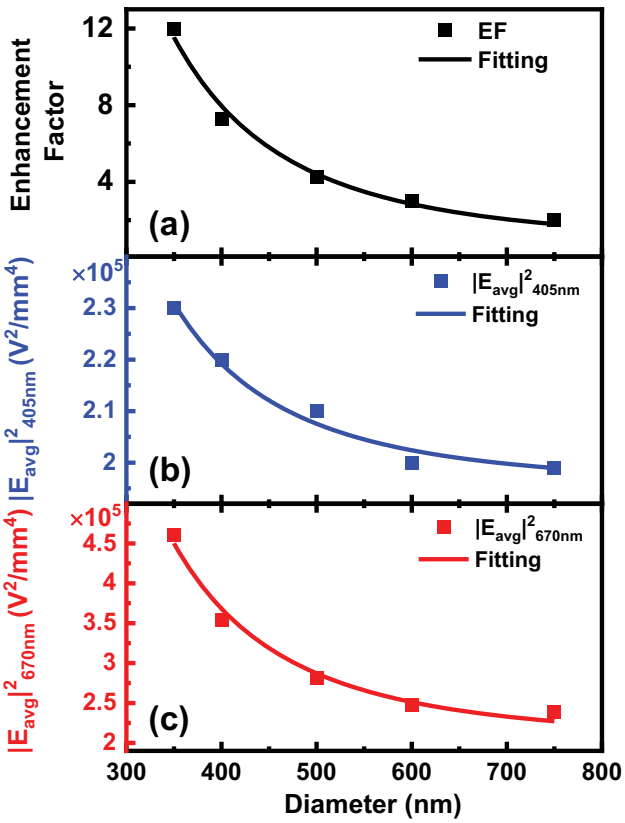

Figure 4: (a) Enhancement factor for each structure to enhance PL intensity of a 1-L MoS_2, and the average E-field intensity of each structure. The numerically calculated local field enhancement of the Au metasurfaces per unit area under the excitation (b) and emission (c) wavelengths (405 and 677 nm), respectively.

the numerical results show that the enhancement factor will reach 23 upon using the nanospheres with the diameter of 200 nm. However, in our experiments, the fabrication of the large-area Au metasurfaces becomes challenging when the diameter of the nanospheres is less than 300 nm. The further improvement of the self-assembly process and precise gap tuning with small nanospheres is still undergoing.

4 Conclusion

In summary, we have demonstrated a simple, cost-effective approach to enhance the PL signal of the monolayer MoS_2. Hexagonal Au metasurfaces were fabricated from the templated masks that were formed by self-assembled polystyrene nanospheres. By transferring the monolayer MoS_2 onto these Au metasurfaces, the PL signal of the monolayer MoS_2 can be significantly enhanced. Under a 405 nm laser beam excitation, the LSPR-enhanced monolayer MoS_2 exhibited a 12-fold increase in PL over a large area. We expect our proposed approach could pave the way

for many potential applications based on plasmon-enhanced 2D TMDCs.

Acknowledgments: The authors acknowledge the assistance of SUSTech Core Research Facilities.
Author contributions: All the authors have accepted responsibility for the entire content of this submitted manuscript and approved submission.
Research funding: This work was supported in part by National Natural Science Foundation of China (Grant No. 62075093 and 61805113), China Postdoctoral Science Foundation (2020M672697), Natural Science Foundation of Guangdong Province (Grant No. 2018A030310224 and 2019A1515110864), Guangdong Innovative and Entrepreneurial Research Team Program (Grant No. 2017ZT07C071), and Shenzhen Science and Technology Innovation Commission (Grant No. GJHZ20180928155207206, JCYJ20170817111349280, and JCYJ20180305180635082). Meng Zhao acknowledges the support from the Agency for Science, Technology and Research (A*STAR) (Grant No. 152700014 and H19H6a0025).
Conflict of interest statement: The authors declare no conflicts of interest regarding this article.

References

[1] Z. L. Ye, T. Cao, K. O'Brien, et al., "Probing excitonic dark states in single-layer tungsten disulphide," *Nature*, vol. 513, pp. 214–218, 2014.
[2] C. T. Yip, T. W. Lo, S. C. Zhu, et al., "Tight-binding modeling of excitonic response in Van Der Waals stacked 2D semiconductors," *Nanoscale Horiz.*, vol. 4, pp. 969–974, 2019.
[3] Y. Ye, J. Xiao, H. L. Wang, et al., "Electrical generation and control of the valley carriers in a monolayer transition metal dichalcogenide," *Nat. Nanotechnol.*, vol. 11, pp. 598–602, 2016.
[4] J. Liu, T. W. Lo, J. Sun, C. T. Yip, C. H. Lam, and D. Y. Lei, "A comprehensive comparison study on the vibrational and optical properties of CVD-grown and mechanically exfoliated few-layered WS_2," *J. Mater. Chem. C*, vol. 5, pp. 11239–11245, 2017.
[5] S. F. Wu, C. M. Huang, G. Aivazian, J. S. Ross, D. H. Cobden, and X. D. Xu, "Vapor-solid growth of high optical quality MoS_2 monolayers with near-unity valley polarization," *ACS Nano*, vol. 7, pp. 2768–2772, 2013.
[6] M. Buscema, D. J. Groenendijk, S. I. Blanter, G. A. Steele, H. S. J. van der Zant, and A. Castellanos-Gomez, "Fast and broadband photoresponse of few-layer black phosphorus field-effect transistors," *Nano Lett.*, vol. 14, pp. 3347–3352, 2014.
[7] M. Y. Li, Y. M. Shi, C. C. Cheng, et al., "Epitaxial growth of a monolayer WSe_2-MoS_2 lateral P-N junction with an atomically sharp interface," *Science*, vol. 349, pp. 524–528, 2015.
[8] S. Mouri, Y. Miyauchi, and K. Matsuda, "Tunable photoluminescence of monolayer MoS_2 via chemical doping," *Nano Lett.*, vol. 13, pp. 5944–5948, 2013.
[9] Y. H. Chang, W. Zhang, Y. Zhu, et al., "Monolayer $MoSe_2$ grown by chemical vapor deposition for fast photodetection," *ACS Nano*, vol. 8, pp. 8582–8590, 2014.
[10] H. Kim, D. H. Lien, M. Amani, J. W. Ager, and A. Javey, "Highly stable near-unity photoluminescence yield in monolayer MoS_2 by fluoropolymer encapsulation and superacid treatment," *ACS Nano*, vol. 11, pp. 5179–5185, 2017.
[11] B. Radisavljevic, A. Radenovic, J. Brivio, V. Giacometti, and A. Kis, "Single-layer MoS_2 transistors," *Nat. Nanotechnol.*, vol. 6, pp. 147–150, 2011.
[12] Z. Yin, H. Li, H. Li, et al., "Single-layer MoS_2 phototransistors," *ACS Nano*, vol. 6, pp. 74–80, 2012.
[13] P. Chen, T. W. Lo, Y. Fan, S. Wang, H. Huang, and D. Lei, "Chiral coupling of valley excitons and light through photonic spin–orbit interactions," *Adv. Opt. Mater.*, vol. 8, 2020, Art no. 1901233.
[14] O. Lopez-Sanchez, D. Lembke, M. Kayci, A. Radenovic, and A. Kis, "Ultrasensitive photodetectors based on monolayer MoS_2," *Nat. Nanotechnol.*, vol. 8, pp. 497–501, 2013.
[15] Z. Peng, X. Chen, Y. Fan, D. J. Srolovitz, and D. Lei, "Strain engineering of 2D semiconductors and graphene: from strain gields to band-structure tuning and photonic applications," *Light Sci. Appl.*, vol. 9, 2020, Art no. 190.
[16] S. Bertolazzi, J. Brivio, and A. Kis, "Stretching and breaking of ultrathin MoS_2," *ACS Nano*, vol. 5, pp. 9703–9709, 2011.
[17] X. Qi, T. W. Lo, D. Liu, et al., "Effects of gap thickness and emitter location on the photoluminescence enhancement of monolayer MoS_2 in a plasmonic nanoparticle-film coupled system," *Nanophotonics*, vol. 9, pp. 2097–2105, 2020.
[18] M. Amani, R. A. Burke, X. Ji, et al., "High luminescence efficiency in MoS_2 grown by chemical vapor deposition," *ACS Nano*, vol. 10, pp. 6535–6541, 2016.
[19] T. Valla, A. V. Fedorov, P. D. Johnson, J. Xue, K. E. Smith, and F. J. DiSalvo, "Charge-density-wave-induced modifications to the quasiparticle self-energy in 2h-$TaSe_2$," *Phys. Rev. Lett.*, vol. 85, pp. 4759–4762, 2000.
[20] S. S. Singha, D. Nandi, and A. Singha, "Tuning the photoluminescence and ultrasensitive trace detection properties of few-layer MoS_2 by decoration with gold nanoparticles," *RSC Adv.*, vol. 5, pp. 24188–24193, 2015.
[21] S. Najmaei, A. Mlayah, A. Arbouet, C. Girard, J. Leotin, and J. Lou, "Plasmonic pumping of excitonic photoluminescence in hybrid MoS_2-Au metasurface," *ACS Nano*, vol. 8, pp. 12682–12689, 2014.
[22] S. Butun, S. Tongay, and K. Aydin, "Enhanced light emission from large-area monolayer MoS_2 using plasmonic nanodisc arrays," *Nano Lett.*, vol. 15, pp. 2700–2704, 2015.
[23] B. Lee, J. Park, G. H. Han, et al., "Fano resonance and spectrally modified photoluminescence enhancement in monolayer MoS_2 integrated with plasmonic nanoantenna array," *Nano Lett.*, vol. 15, pp. 3646–53, 2015.
[24] M. G. Lee, S. Yoo, T. Kim, and Q. H. Park, "Large-area plasmon enhanced two-dimensional MoS_2," *Nanoscale*, vol. 9, pp. 16244–16248, 2017.
[25] S. Y. Choi, C. T. Yip, G. Li, et al., "Photoluminescence enhancement in few-layer WS_2 films via Au nanoparticles," *AIP Adv.*, vol. 5, 2015, Art no. 067148.
[26] Y. Kang, S. Najmaei, Z. Liu, et al., "Plasmonic hot electron induced structural phase transition in a MoS_2 monolayer," *Adv. Mater.*, vol. 26, pp. 6467–6471, 2014.

[27] K. C. Lee, Y. H. Chen, H. Y. Lin, et al., "Plasmonic gold nanorods coverage influence on enhancement of the photoluminescence of two-dimensional MoS_2 monolayer," *Sci. Rep.*, vol. 5, 2015, Art no. 16374.
[28] G. M. Akselrod, T. Ming, C. Argyropoulos, et al., "Leveraging nanocavity harmonics for control of optical processes in 2D semiconductors," *Nano Lett.*, vol. 15, pp. 3578–3584, 2015.
[29] T. W. Lo, Q. Zhang, M. Qiu, et al., "Thermal redistribution of exciton population in monolayer transition metal dichalcogenides probed with plasmon–exciton coupling spectroscopy," *ACS Photonics*, vol. 6, pp. 411–421, 2019.
[30] M. Decker and I. Staude, "Resonant dielectric metasurface: a low-loss platform for functional nanophotonics," *J. Opt.*, vol. 18, 2016, Art no. 103001.
[31] S. Kruk and Y. Kivshar, "Functional meta-optics and nanophotonics govern by mie resonances," *ACS Photonics*, vol. 4, pp. 2638–2649, 2017.
[32] A. Vaskin, J. Bohn, K. E. Chong, et al., "Directional and spectral shaping of light emission with mie-resonant silicon nanoantenna arrays," *ACS Photonics*, vol. 5, pp. 1359–1364, 2018.
[33] S. Liu, A. Vaskin, S. Addamane, et al., "Light-emitting metasurface: simultaneous control of spontaneous emission and far-field radiation," *Nano Lett.*, vol. 18, pp. 6906–6914, 2018.
[34] A. F. Cihan, A. G. Curto, S. Raza, P. G. Kik, and M. L. Brongersma, "Silicon mie resonators for highly directional light emission from monolayer MoS_2," *Nat. Photonics*, vol. 12, pp. 284–290, 2018.
[35] H. Chen, S. Nanz, A. Abass, et al., "Enhanced directional emission from monolayer WSe_2 integrated onto a multiresonant silicon-based photonic structure," *ACS Photonics*, vol. 4, pp. 3031–3038, 2017.
[36] Y. Zhang, W. Chen, T. Fu, et al., "Simultaneous surface-enhanced resonant Raman and fluorescence spectroscopy of monolayer $MoSe_2$: determination of ultrafast decay rates in nanometer dimension," *Nano Lett.*, vol. 19, pp. 6284–6291, 2019.
[37] A. D. Johnson, F. Cheng, Y. Tsai, and C. Shih, "Giant enhancement of defect-bound exciton luminescence and suppression of band-edge luminescence in monolayer WSe_2-Ag plasmonic hybrid structures," *Nano Lett.*, vol. 17, pp. 4317–4322, 2017.
[38] G. Cossio and E. T. Yu, "Zeta potential dependent self-assembly for very large area nanosphere lithography," *Nano Lett.*, vol. 20, pp. 5090–5096, 2020.
[39] X. Fang, C. Zheng, Z. Yin, et al., "Hierarchically ordered silicon metastructures from improved self-assembly-based nanosphere lithography," *ACS Appl. Mater. Interfaces*, vol. 12, pp. 12345–12352, 2020.
[40] T. Liang, S. Xie, W. Fu, et al., "Synthesis and fast transfer of monolayer MoS_2 on reusable fused silica," *Nanoscale*, vol. 9, 2017, Art no. 6984.
[41] H. Li, Q. Zhang, C. C. R. Yap, et al., "From bulk to monolayer MoS_2: evolution of Raman scattering," *Adv. Funct. Mater.*, vol. 22, pp. 1385–1390, 2012.
[42] P. Tonndorf, R. Schmidt, P. Böttger, et al., "Photoluminescence emission and Raman response of monolayer MoS_2, $MoSe_2$, and WSe_2," *Opt. Express*, vol. 21, pp. 4908–4916, 2013.
[43] W. Gao, Y. H. Lee, R. Jiang, J. Wang, T. Liu, and X. Y. Ling, "Localized and continuous tuning of monolayer MoS_2 photoluminescence using a single shape-controlled Ag nanoantenna," *Adv. Mater.*, vol. 28, pp. 701–706, 2016.
[44] A. Splendiani, L. Sun, Y. Zhang, et al., "Emerging photoluminescence in monolayer MoS_2," *Nano Lett.*, vol. 10, pp. 1271–1275, 2010.
[45] G. Sun, J. B. Khurgin, and R. A. Soref, "Plasmonic light-emission enhancement with isolated metal nanoparticles and their coupled arrays," *J. Opt. Soc. Am. B*, vol. 25, pp. 1748–1755, 2008.
[46] K. F. Mak and J. Shan, "Photonics and optoelectroncis of 2D semiconductor transition metal dichacogenides," *Nat. Photonics*, vol. 10, pp. 216–226, 2016.
[47] K.-D. Park, T. Jiang, G. Clark, X. Xu, and M. B. Raschke, "Radiative control of dark excitons at room temperature by nano-optical antenna-tip Purcell effect," *Nat. Nanotechnol.*, vol. 13, pp. 59–64, 2018.
[48] F. J. Wendisch, R. Oberreiter, M. Salihovic, M. S. Elsaesser, and G. R. Bourret, "Confined etching within 2D and 3D colloidal crystals for tunable nanostructured templates: local environment matters," *ACS Appl. Mater. Interfaces*, vol. 9, pp. 3931–3939, 2017.

Supplementary Material: The online version of this article offers supplementary material (https://doi.org/10.1515/nanoph-2020-0672).

Detailed description of SEM images of Au metasurfaces, AFM images of nontransferred 1-L MoS_2 and Au metasurface, PL spectra of the 1-L MoS_2 on Au metasurfaces, and calculation of average E-field intensity.